IEEE Access
Multidisciplinary | Rapid Review | Open Access Journal

Received 6 March 2024, accepted 5 April 2024, date of publication 9 April 2024, date of current version 18 April 2024.

Digital Object Identifier 10.1109/ACCESS.2024.3386549

APPLIED RESEARCH

Design, Analysis, and Implementation of a 3-DOF Spherical Parallel Manipulator

MOHAMED DJENNANE[1], SEIF EDDINE CHEHAIDIA[1], CHOUITER YAKOUB[1], KHAWLA MESBAH[1], MANSOUR ALJOHANI[2], AND MOHMED I. MOSAAD[2], (Senior Member, IEEE)

[1]École Nationale Polytechnique de Constantine, Constantine 25000, Algeria
[2]Yanbu Industrial College (YIC), Royal Commission Yanbu Colleges and Institutes, Yanbu 46452, Saudi Arabia

Corresponding authors: Mohmed I. Mosaad (m_i_mosaad@hotmail.com) and Seif Eddine Chehaidia (seifeddinechehaidia@yahoo.fr)

ABSTRACT The agile eye is classified as a 3-degrees of freedom (DOF) type 3-RRR spherical parallel mechanism (SPM) designed to replicate the movement patterns seen in the human eye. The end organ exhibits a range of motion inside a cone of vision spanning 140°, with a twist tolerance of ±30°. Additionally, the mechanism can achieve angular velocities exceeding 1000 °/s and angular accelerations surpassing 20 °/s^2. The objective of this research is to conduct a comprehensive examination of the direct and inverse kinematics of the spatial parallel manipulator (SPM) on a manipulator. The purpose of doing a kinematic analysis on the manipulator is to enhance the design optimization process, accurately determine the dimensions of all components, and improve the functionality of the computer-aided design (CAD) system. This study aims to ensure the efficient operation of the SPM and maximize its available workspace. Additionally, this study enables the achievement of a high level of stiffness inside the workspace and the establishment of clearly comprehensible limits for the workspace. Moreover, it facilitates the precise control of the SPM. An evaluation is conducted to assess the efficacy of the existing technique by comparing its outputs with those obtained from a virtual reality simulation using the commercially available software CopeliaSim. The control mechanism described in the present paper demonstrates a surplus in the resolution of precision problems while ensuring competitiveness at a controlled cost. The implementation of the robot revealed the effectiveness of the design approach adopted by recording an error of no more than 1%.

INDEX TERMS Mechatronics, precision engineering, spherical parallel manipulator, Euler angles, optimization, implementation.

NOMENCLATURE

$\mathbf{U_i}$	Unit vectors directed along the axes of the actuators A_i.
γ	Angle between the actuators axes A_i.
$\mathbf{V_i}$	Unit vectors directed along the axes of the pivot joints connected to the end effectors B_i.
$\mathbf{W_i}$	Unit vectors directed along the axes of the intermediate pivot joints C_i.
α_1	Angle between A_i and C_i.
α_2	Angle between C_i and B_i.
β	Angle between the normal of the base and the actuators axes A_i.
θ	Angle of rotation motor.
$\mathbf{J}$	Jacobean matrices of the manipulator.
$\mathbf{K}$	Dexterity.
$\|\|.\|\|$	Euclidean norm of the matrix.
ζ	Reciprocal number.
η	Global index for the optimization of robot.
$\mathbf{W}$	Working space of the.
$\mathbf{kappa_{min}}$	Minimum dexterity.
$\boldsymbol{V_i}$	Initial state vector of the manipulator.
$\mathbf{R}$	Rotation matrix.

The associate editor coordinating the review of this manuscript and approving it for publication was Binit Lukose.

$\mathbf{W_1}, \mathbf{W_2}, \mathbf{W_3}$ Projections of W_i vectors in the fixed frame.

I. INTRODUCTION

After the fascinating success of robots for industrial applications, they know a massive evolution by touching all live fields [1], [2]. The Agile Eye robot is a 3 degree of freedom spherical parallel mechanism (SPM). It is intended to function as an orientation device for cameras, mirrors, and lasers. The robot is designed to operate within a significantly larger working space than the human eye while maintaining high precision and dynamic performance. Numerous research studies have been conducted on the agile eye, resulting in the emergence of various parallel manipulator models, such as the simple SPM, compact SPM, simplified SPM a 2 DOF, and coaxial SPM [3], [4], [5], [6].

Errors are introduced into the kinematics of parallel robots as a result of manufacturing procedures. It is necessary to ascertain the parameters that can effectively minimize parasitic displacements. Several methodologies have been given in the literature to address the kinematic analysis of serial manipulators. However, it is worth noting that these conventional methods are not applicable to the analysis of the SPM. In this particular scenario, advanced robotics methods are employed. The dynamic model of the parallel agile eye robot was initially proposed by [7]. Regarding the modeled design, a symmetrical shoulder structure is proposed. This structure proves its efficiency and is retained as a main used structure for the next published research. Several methods can be cited, such as the geometrical method, the screw theory, and the Euler angles [8], [9], [10], [11], [12], [13]. Gosselin and Hamel performed a kinematic optimization to determine the dimensional parameters of the prototype that would provide the best overall accuracy [3]. Kong and Gosselin proposed an alternative formulation of the kinematic equations of the agile eye [14]. A regular cube in the input space, without singularity, is proposed to facilitate the control of the Agile Eye. However, the use of a regular cube results in high inertia compared to spherical geometry. Bonev et al. (year) provided that the four assembly modes, which correspond to the direct kinematics of the agile eye, exhibit a straightforward and direct correlation with the eight working modes, representing the solutions to the inverse kinematics [12]. Chablat and Wenger conducted an optimization study on two parallel mechanisms to enhance their stiffness and reduce the number of moving components [15]. Kuo and Legnani found the solutions of the direct and inverse kinematics of the parallel orientation mechanism with three degrees of freedom. They derived solutions for these kinematic problems using geometrical reasoning and offered theoretical proof for their findings. Cammarata et al. elucidated the impact of stress errors resulting from the manufacturing process of rotation axes on the inverse kinematic model of the Agile Eye [16]. A closed-form model is derived from the nominal inverse kinematic model to incorporate geometric imperfections on the axes of rotating joints. The kinematic study of this mechanism is conducted utilizing the compliance matrix approach, whereby two distinct forms of compliant rotary joints are assessed alongside three inputs. The inputs in question can be either forces or displacements, acting independently. The analysis conducted in Ref. [17] yields equations that establish the relationship between the input forces/displacements and the displacement of the moving platform. The expressions above are utilized to acquire the necessary inputs for executing a rotational trajectory of the mobile platform. In the course of this operation, extraneous displacements are computed. The kinematic analysis expressions have been empirically validated to demonstrate decreased parasitic displacements. In Ref. [18], a 3D printed manipulator of 3 DOF is implemented. Regarding its mechanical design, the structure is simple and does not require advanced manufacturing and high-cost machines or components. Experimental tests conducted on the robot show the effectiveness of the design. In Ref. [19], the authors present the concept of spherical robots and their driving mechanism. It underlines the importance of energy consumption in the trajectory planning of spherical robots operating outdoors. The major contribution of the paper is the proposition of an improved algorithm that aims to minimise both energy consumption and trajectory length. However, the study is limited to design, and no experimental prototypes have been produced. It is, therefore, difficult to verify the applicability of the algorithm. Schröder et al. [20] conducted a study in which they developed and executed a spherical robot, examining the efficacy of three control laws for position control: Villela, IPC, and Reinforcement Learning. One notable aspect of this article is the use of rapid prototyping, a technique renowned for its precision, time efficiency, and comparatively affordable nature. However, there was a large error between simulation and reality over $\pm 5\%$; although the trend is similar, more work on accuracy is required. In Ref [21], the authors present a new spherical robot equipped with a cable transmission mechanism designed specifically to replace conventional gears, thus eliminating the effects of gear backlash, reducing its mass, and lowering its cost. As for control, a hierarchical finite-time adaptive sliding mode strategy (FAHSMC) is proposed to minimise convergence time. For velocity control, a hierarchical sliding mode controller (HSMC) and a nonlinear disturbance observer based on a tracking differentiator (TD) are developed. However, no study has been carried out on the impact of chatering phenomena, which is known to weaken the robot's components over time due to the commutative nature of the controller. In [22], a spherical robot with a suspended pendulum is presented. The aim of the study was to save energy to improve endurance during sensing tasks. A feedback controller based on the optimisation of regenerative damping parameters using particle swarm optimisation. These approaches reduce energy consumption by 44%. However, the result would be more valuable if

it were experimental or validated by a certified simulator. Sagsoz and Eray [23], presented the design and kinematics analysis of a mechanically coupled two spherical robots for outdoor tasks. The structural design was simple, offering the advantage of the ease of manufacturing, with a rigid coupling to enhance the stability if the robot. The obtained results is satisfactory, however, the use of elastic coupling gives more stability and overcome the non-plane nature of fields. Arif et al. [24], presented the design of a high-torque spherical amphibious robot equipped with twin eccentric pendulums, providing land and sea traction tasks. Tests carried out on the experimental prototype show the effectiveness of the design and its ability to meet the requirements of the initially predefined specifications. Bu et al. [25] present the design of a mobile spherical robot using four four-wheel omnidirectional patterns. A motion controller with a slipping observer is also implemented to increase the robot's precision. A self-balancing structure based on a spherical robot is proposed in [26]. Camera-orienting agile eye robot is proposed by [27]. The use of 3D orientation ensured by the parallel spherical structure of the robot enhances the performance of active vision. In addition, detailed kinematic analysis of agile eye parallel spherical robot is presented in [28]. The design and development of a spherical parallel robot is proposed by [29], ensuring as application domain the laser pointing tasks. From a mechanical design point of view, the viro structure proposed by [27] is adopted. DC motors were used, and the motors were controlled by EtherCAT. The major drawback is the robot's accuracy, with significant error due to the imprecision of the joints produced by an additive manufacturing process. Wu and Bai [30], proposes the design and carry out a 3DOFs spherical parallel robot based on reconfigured with four–bar linkages. The proposed design is of a hight accuracy since a gear transmission is used, one can also observe the robustness of the proposed design. However, regarding the improvement behind the use of the proposed linkage does not contribute to the dynamic behaviour improvement of the robot compared to existing one. The present paper presents an Agile Eye device with three degrees of freedom. These properties enable a high level of rigidity over the whole range of motion and clearly defined limits inside the workspace, facilitating user comprehension. The use of the Euler angle technique in this study is justified by its earlier application by other researchers [3], [4], [5], [6], [7]. The rotation matrices will be employed to determine the relationship between the orientation of the mobile frame and the angles of the three motors. The Agile Eye's direct and inverse problems will be examined through a kinematic analysis, with the objective of controlling the manipulator to enable the robot to track a predetermined trajectory accurately. As a summay the main contribution of the present paper are:

- Design and implementation of a multifunction parallel spherical robot based on rapid prototyping.
- The primary objective is to present a novel application involving the utilization of a laser to follow a precisely defined trajectory, which is then regulated by programs written in G code.
- Based on pattern recognition, the proposed spherical robot can ensure either pattern recognition or tracking.
- The obstacle avoidance is also included for the lazer application of the robot.
- Rapid prototyping optimization is conducted is order to overcome the reported precision problem in existing bibliography.

In the rest of the paper, the mechatronic design of the robot is given in Section II. The kinematic analysis is then presented in Section III. Results and discussion are presented In Section IV. Finally, the main conclusions are given in Section V.

II. MECHATRONIC DESIGN DESCRIPTION

This robot is designed to perform the LASIK technique, which is a corneal refractive surgery commonly used to correct the eyesight of patients suffering from myopia, hypermetropia, astigmatism, and presbyopia using lasers. A spherical architecture is adopted for this purpose. To achieve this, taking into account the specifications requiring the execution of a precise circle, an initial design was drawn up using Solidworks software. It consists of a fixed hexagonal base, shown in Fig. 1. The choice of this geometry is justified by the ease with which the various axes can be set up while respecting the constraint of the center of rotation of the robot. It will also make installing the motor supports at equal angles easier while minimizing the material used. As a result, the design could be streamlined and its cost minimized. The material chosen was Medium-density fibreboard (MDF), and the removal of the material ensured its production. The motor support shown in Fig. 1 is intended to support the stepper motor, and the material chosen was ABS made using additive manufacturing.

In the same way, the proximal arms, distal arms, articulation joints, and end effector platforms were manufactured. The spherical geometry is ensured thanks to the addition of the arms by the joints supposedly housed in the 625-2RS bearings. The end effector precision has been enhanced by including spherical hubs in its platform, which support the laser pointer. The Ultimaker 2ì Extended 3D printer is used; it supports PLA, ABS, or CPE filaments. Before producing the robot parts, printing parameters are optimized to ensure the production of highly precise components. The best-obtained roughness is 20 μm. The manufacturing parameters were nozzle diameter 0.6 mm; filament diameter 2.85 mm, print speed of 300 (mm/s); thin profile, grid fill pattern, fill density of 60ì, and ABS material.

In order to verify the resistance of the design, a Finite Element Analysis (FEM) was carried out. Following the standard methodology, after importing the CAD model and material assignment, boundary conditions are introduced where the robot frame is considered as fixed geometry. Roller-type boundary conditions are presented at the joints. As for loads,

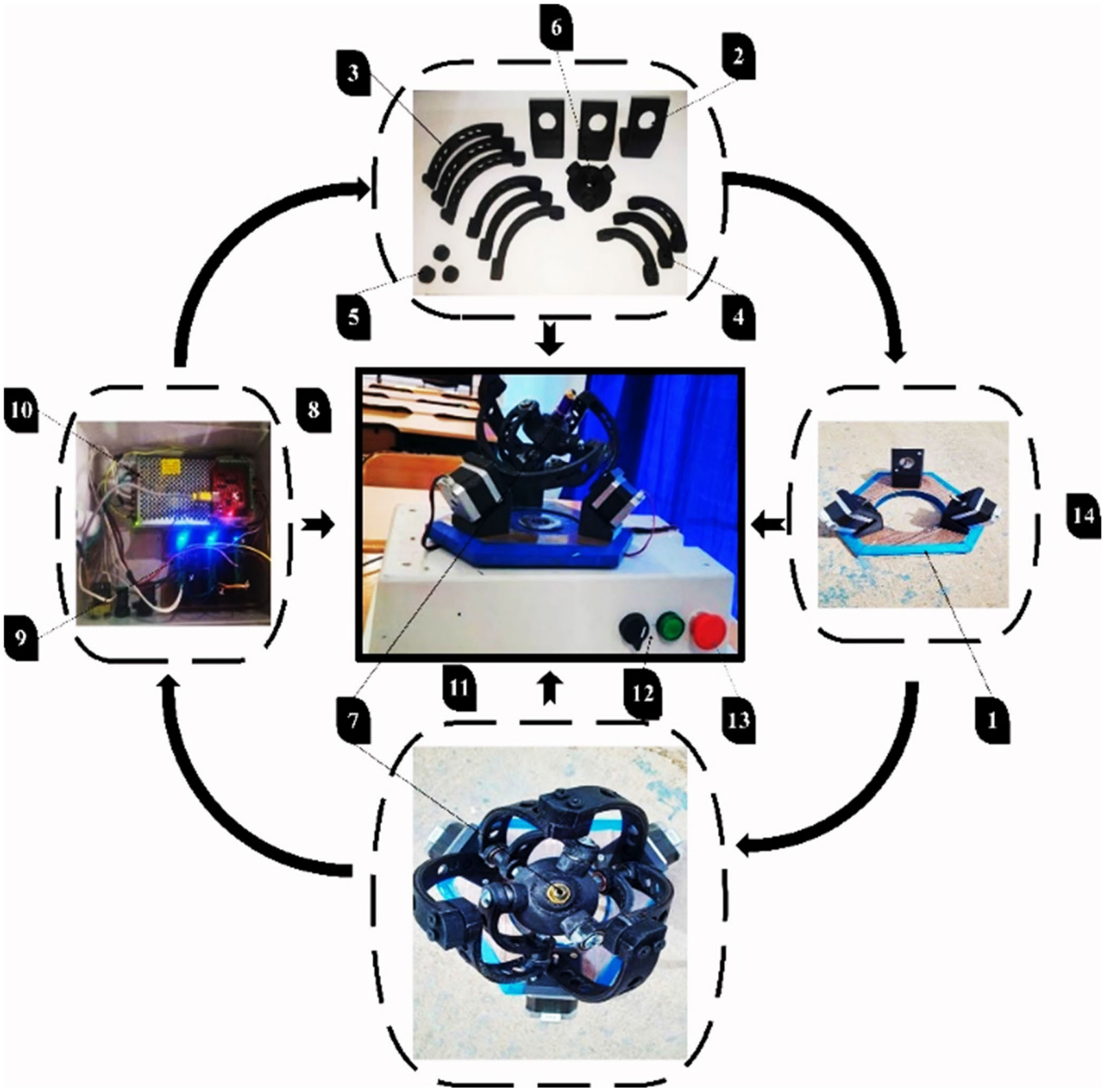

(1) Robot frame; (2) Motor support; (3) proximal arms; (4) Distal arm; (5) articulation joints; (6) End effector platform; (7) Laser pointer, (8) MAC 3 card, 4 axis ; (9) Driver TB6600 ; (10) Power supply S-120-12 ; (11) Control panel ; (12) Rotary on/off switch ; (13) Emergency stop ; (14) Stepper Motor Nema 17.

FIGURE 1. Design description.

stepper motor weight forces are considered on the support; torques are considered for connecting the stepper motor shaft and proximal arm. Bearing load and gravity are also considered. For model discretization, a standard 2 mm mesh with 16 Jacobian points is supposed to perform the FEA. The number of nodes was 937784, and the number of elements was 671892, as shown in Fig. 2 (a). The maximum von mises stress shown in Fig. 2 (b) does not exceed 14.31 N/m^2, concentrated as expected at the supports and end effector frame. This will allow the ABS to be used safely. The static displacement obtained is also very satisfactory and does not exceed 4.43 $\times$ 10.5 mm, as seen in Fig. 2 (c). Fig. 2 (d) shows the static strain, which was negligible given the low displacement, displaying values of $\times 10^{-5}$ (mm).

Concerning the control system of the present robot, it was decided to use the Mac 3 four-axis card configured to operate at a frequency of 25 kHz. In fact, TB 6600 drivers are used to pilot the stepper motors. The G code is then communicated to the card via the Mac 3 graphical user interface. The circuit is supplied by an S-120-12 power supply, as shown in Fig. 3.

As for wiring the Mac3 microcontroller to the driver, the so-called common anode method is used. The positive pulse

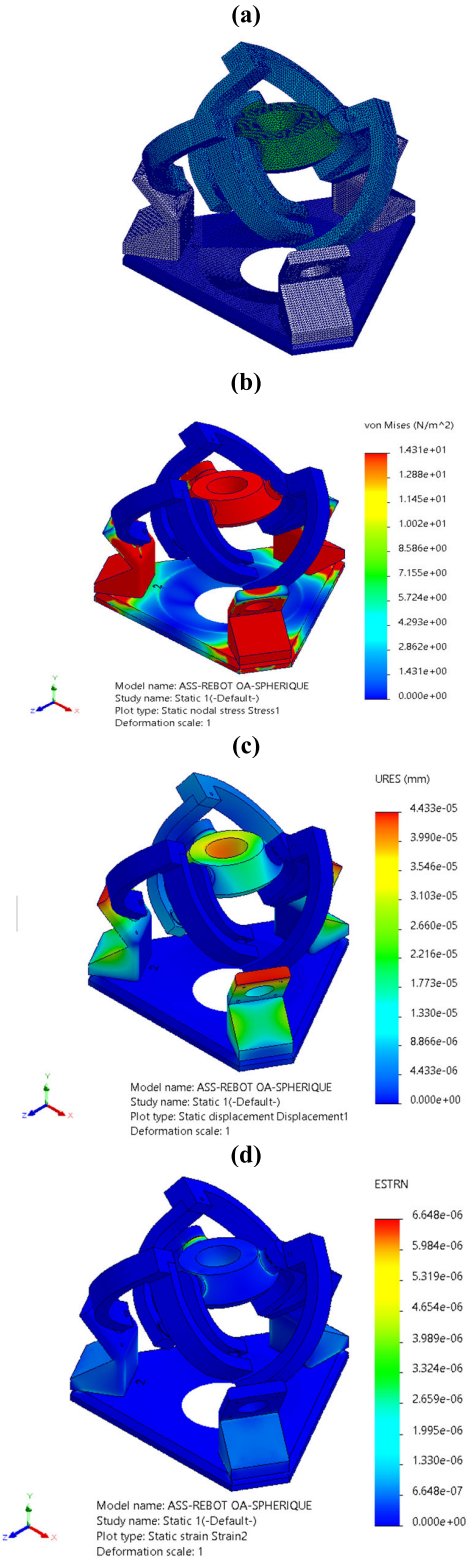

FIGURE 2. Finite element Analysis, (a) Model meshing, (b) Von Mises stress, (c) Displacement, d) Strain.

(PUL+) and plus direction (DIR+) of each axis are all connected to (5V), while the minus pulse (PUL-) is connected to the axis pulse (XP; YP; ZP), and the minus direction (DIR-) is related to the axis direction (XD; YD; ZD).

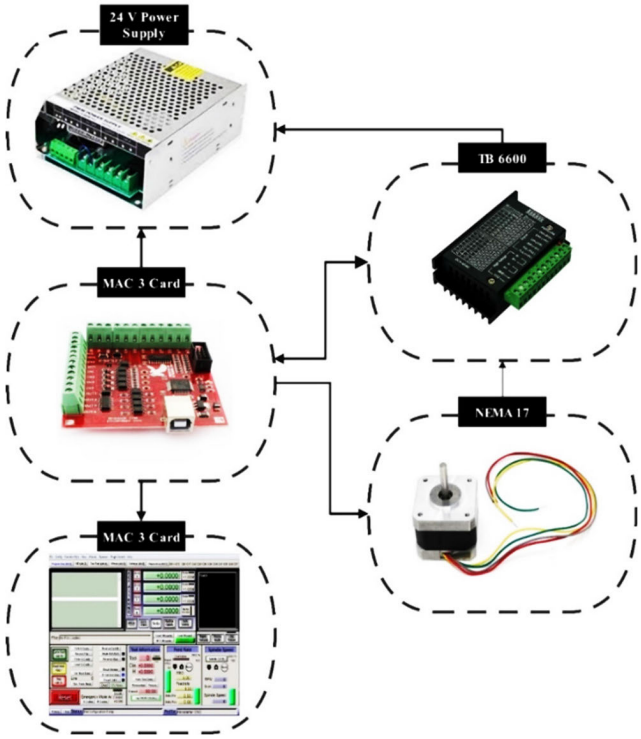

FIGURE 3. Implementations of the control unit of the robot.

Fig. 4 (a) shows the control design of the robot where the microcontroller is wired with a single driver (the X-axis driver) using the common anode method. Fig. 4 (b) shows the wiring of the three drivers with the microcontroller. Fig. 4 (c) shows the wiring of the three drivers with the microcontroller; note that the A axis is unused, given the 3-axis architecture design is presented previously. Regarding the cabling of the drivers with the stepper motors, the two fils of phase A are connected to A- and A+, and the two fils of phase B are connected to B- and B+ as shown in figure c. Finally, the drivers are connected to the power supply S 120-12. The I/O of the microcontroller allows the implementation of the emergency stop circuit E stop, which will suspend the current signal feeding the drivers and motors, where the input of the power supply is connected with the power source and its output is connected with the driver: V+ with VCC and V- with GND, as shown Fig. 4 (d).

III. KINEMATIC MODELING AND ANALYSIS

To ensure the proper functioning of an SPM, the architecture of the manipulator must be such that the axes of the nine pivot joints A_i, B_i, and C_i {i=1, 2, 3 intersect at a common point called the robot center of rotation, as shown Fig. 5. In addition, the angles β and γ are needed to define the geometry of the base; the motor support and the end effector as shown in Fig. 6.

of the manipulator must be such that the axes of the nine pivot joints A_i, B_i, and C_i {i=1, 2, 3} intersect at a common point called the robot center of rotation, as shown by Fig. 6.

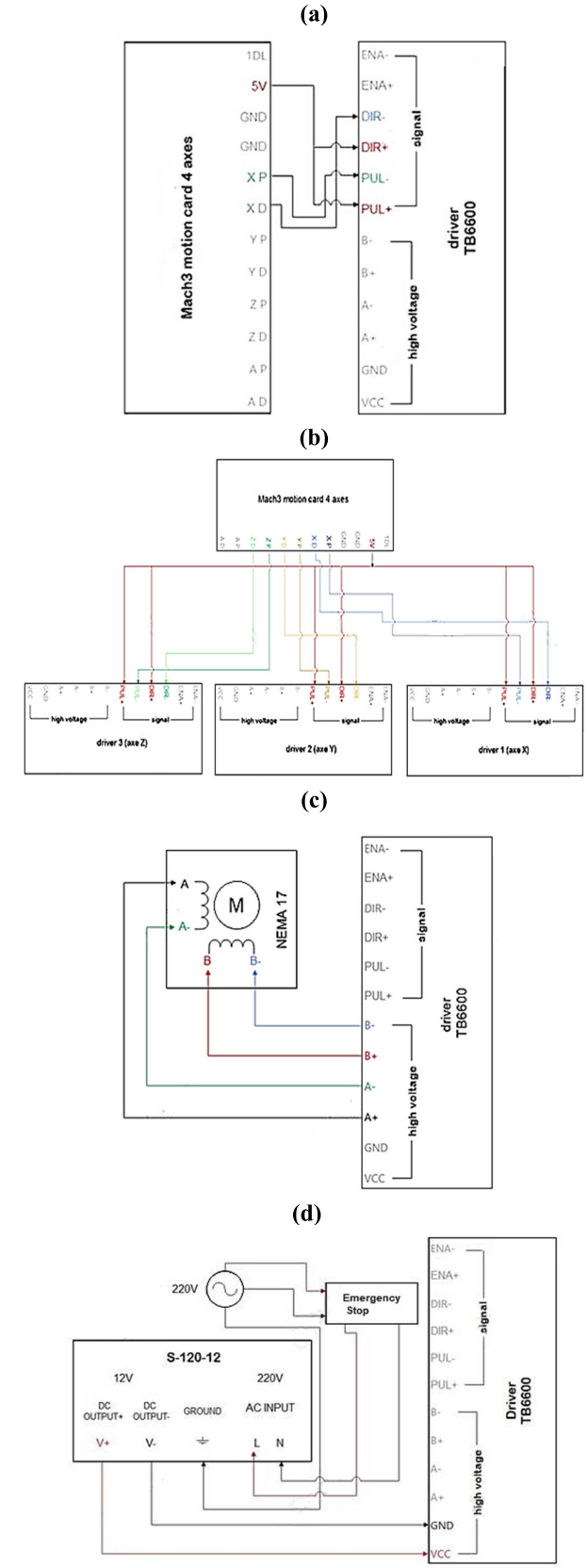

FIGURE 4. Hardware wiring, (a) Driver/ MAC 3 card, (b) All used driver/MAC 3 card, (c) stepper motor/driver, (d) Power supply/driver, including the emergency stop loop.

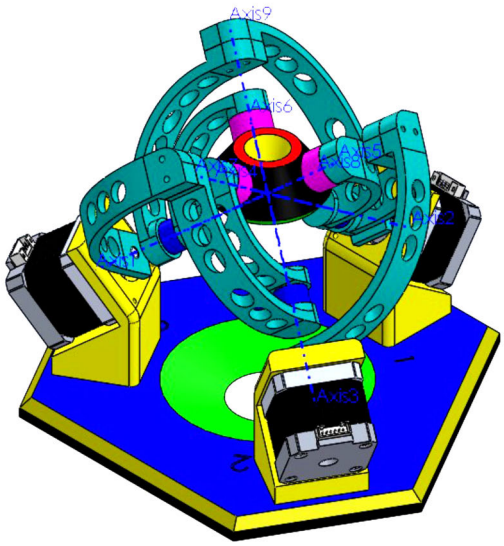

FIGURE 5. Robot center of rotation.

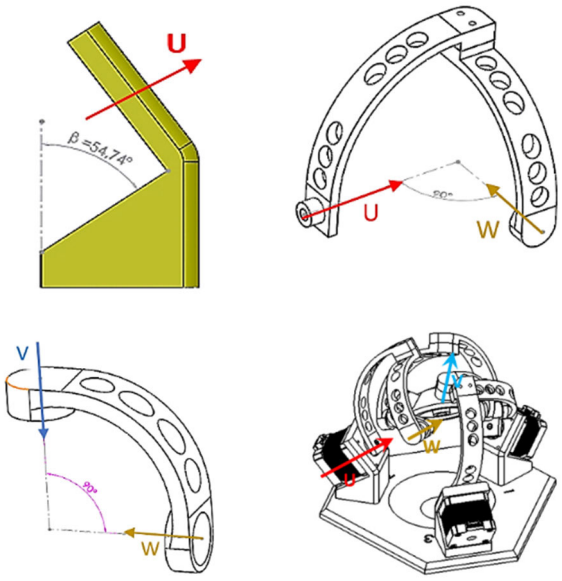

FIGURE 6. Robot axes.

In addition, the angles β and γ are needed to define the geometry of the base; the motor support and the end effector as shown in Fig.6. However, these two angles are dependent; the relationship that connects the angles β and γ is expressed as follows:

$$\sin(\beta) = \frac{2}{\sqrt{3}}.\sin(\frac{\gamma}{2}) \tag{1}$$

In order to ensure the correct design, a geometrical optimization of the agile eye robot was carried out. The angles $\alpha 1$, $\alpha 2$, and γ that result in the highest performance indices, guaranteeing excellent precision and a big workspace, are determined accordingly [31]. Considering J and K, which are the Jacobean matrices of the manipulator, such as [32]:

$$\mathbf{J}\omega + \mathbf{K}\dot{\theta} = 0 \tag{2}$$

TABLE 1. Units for magnetic properties.

Architectural design	γ(°)	α_1(°)	α_2(°)
A	90	90	90
B	120	120	90
C	105	90	105
D	83	90	90

$$\mathbf{J} = \begin{bmatrix} (W_1 x V_1)^T \\ (W_2 x V_2)^T \\ (W_3 x V_3)^T \end{bmatrix} \tag{3}$$

$$\mathbf{K} = \begin{bmatrix} W_1 x U_1 . V_1 & 0 & 0 \\ 0 & W_2 x U_2 . V_2 & 0 \\ 0 & 0 & W_3 x U_3 . V_3 \end{bmatrix} \tag{4}$$

Salisbury and Craig [33], defined the dexterity noted K of a manipulator as the kinematic precision of the manipulator as follows:

$$\mathbf{K} = \left\| -\mathbf{K}^{-1} \mathrm{J} \right\| \left\| -\mathbf{J}^{-1} \right\| ; 1 \leq \mathbf{K} < \infty \tag{5}$$

where ||. || is the Euclidean norm of the matrix, given by (6), as follows:

$$\|\mathrm{A}\| = \sqrt{\mathrm{tr}\left(\mathrm{A}^{\mathrm{T}} \mathrm{WA}\right)}; \mathrm{W} = \frac{1}{\mathrm{n}} . \mathrm{Itr}\left(\mathbf{A}\right) = \sum_{\mathrm{i}=1}^{\mathrm{n}} \mathrm{a_{ii}} \tag{6}$$

where n is the dimension of the matrix A and I is the n×n identity matrix. For the present design analysis, the reciprocal number ζ is used, such as:

$$\zeta = \frac{1}{\mathrm{K}}; \quad 0 \leq \zeta \leq 1 \tag{7}$$

Dexterity varies depending on the configuration and geometric parameters of the robot. A manipulator with a ζ close to 1 is a manipulator that has high kinematic accuracy is when ζ is zero. The manipulator is in a singular configuration (the end effectors remain locked in a single direction). Manipulators that can reach at least one configuration where ζ equals one are called isotopic manipulators [21]. Dexterity is a local performance index; a global index for the optimization of robot manipulators denoted η is used and expressed by (8), such as [34]:

$$\eta = \frac{\int \zeta d\mathrm{W}}{\int \mathrm{dW}} \tag{8}$$

where W is the working space of the manipulator.

The indices above quantify the total kinematic performance of the manipulator and only depend on the architecture. Gosselin and Hamel [3], studied several cases to find the optimal angles for an optimal architecture of the Agile Eye robot manipulator, which summary is given in Table 1). Based on the aforementioned methodology, it was concluded that architecture A is the most optimal; it has the highest overall performance index η =0.81, with a minimum dexterity, $\mathrm{kappa_{min}} = 0.51$. Finally, β is the angle between the base normal and the motor axes calculated by (1), leading to $B = 54.74°$.

The end effector can be pointed in a 140° cone of vision with ± 30 (deg) in torsion. Using the simulation on CoppeliaSim, It was found that the Euler angles vary in the interval [-70,70]. This working space largely exceeds that of the human eye, which is 44 ± 7.2° in adduction, 44.2 ± 6.8° in abduction, 27.9 ± 7.6° in elevation, and 47.1 ± 8.0° in depression [35]. In Figure 3, the (O, U_1, U_2, U_3) frame is the fixed one, and (O, $\mathbf{V_1}$, $\mathbf{V_2}$, $\mathbf{V_3}$) is the mobile frame. To find the relationship between the rotation angles of the motors and the position of the end member A through the mobile frame, the rotation matrix allows the detection of the orientation of the frame after 3 successive rotations based on Euler angles.

For simplification purposes, the roll Pitch and Yaw angles represent three successive rotations about the axes of the fixed **XYZ** coordinate system with angles α, β, γ, respectively, as shown in Fig.8. In addition, it is noticed that for each possible frame rotation, there are unique angles α, β and γ.

To find the final rotation matrix of roll, pitch, yaw **XYZ** (α, β, γ), one must multiply the partial rotation matrices successively with an inverse order because, unlike the classical Euler angles, which are around the axes of the resulting frames of the previous rotation (Fig. 9), all rotations are around the fixed frame.

So, it is easily deduced that the roll, pitch, yaw **XYZ** (γ, β, α), and Euler **ZYX** (α, β, γ)are coincident. The rotation matrix is given by (9), (10), shown at the bottom of the next page, such as in (9) and (10).

The detailed expression is given by (11), shown at the bottom of the next page, such as in (11).

The solution of the mathematical equations obtained by modeling the problem leads to the direct and inverse kinematics of the manipulator. In order to orientate a vector (12), such as:

$$\mathbf{V_i} = \mathrm{R} . \mathbf{V_i}' \tag{12}$$

$\mathrm{V_i}$ presents the vector as the initial state of the manipulator before the rotations.

In the initial state of the manipulator, all the motor angles θ_i and the angles roll, pitch, and yaw XYZ (γ, β, α) are zero. We take counterclockwise as the positive direction for its angles. The projection of the unit vectors of the moving benchmarks into the fixed frame in the initial state of the manipulator gives:

$$\mathbf{V}_1^{'} = \begin{bmatrix} 0 \\ -1 \\ 0 \end{bmatrix}, \mathrm{V}_3^{'} = \begin{bmatrix} -1 \\ 0 \\ 0 \end{bmatrix}, \mathbf{V}_1^{'} = \begin{bmatrix} 0 \\ 0 \\ -1 \end{bmatrix} \tag{13}$$

By using (9) and the rotation matrix provided in (12), it is possible to efficiently generate the synthesis of Vi (γ, β, α) =[V1, V2, V3] as:

$$\mathbf{V}_1 = \begin{bmatrix} \sin(\alpha)\cos(\gamma) - \cos(\alpha)\sin(\beta)\sin(\gamma) \\ -\cos(\alpha)\cos(\gamma) - \sin(\alpha)\sin(\beta)\sin(\gamma) \\ -\cos(\beta)\sin(\gamma) \end{bmatrix} \tag{14}$$

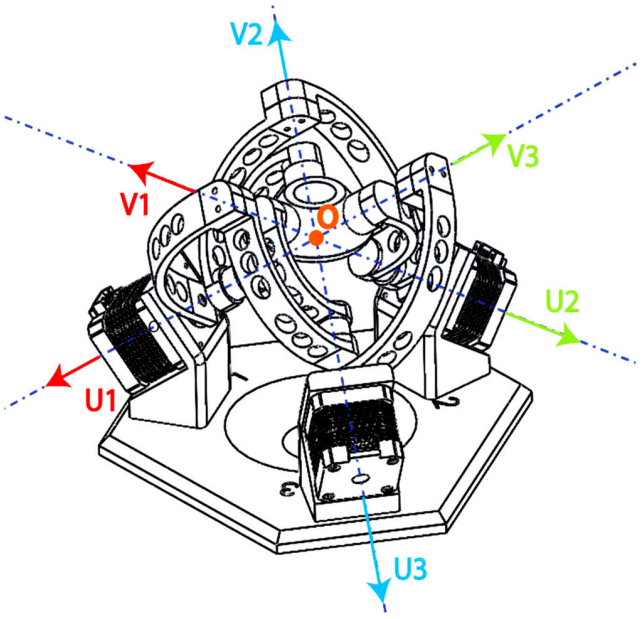

FIGURE 7. Fixed and mobile frames of the manipulator.

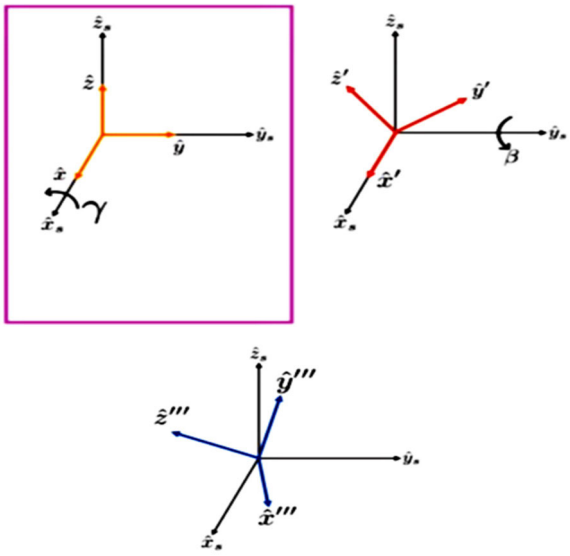

FIGURE 8. Roll, Pitch, Yaw XYZ (α, β, γ).

$$\mathbf{V}_2 = \begin{bmatrix} -\sin(\alpha)\sin(\gamma) - \cos(\alpha)\sin(\beta)\cos(\gamma) \\ -\cos(\alpha)\sin(\gamma) - \sin(\alpha)\sin(\beta)\cos(\gamma) \\ -\cos(\beta)\cos(\gamma) \end{bmatrix} \quad (15)$$

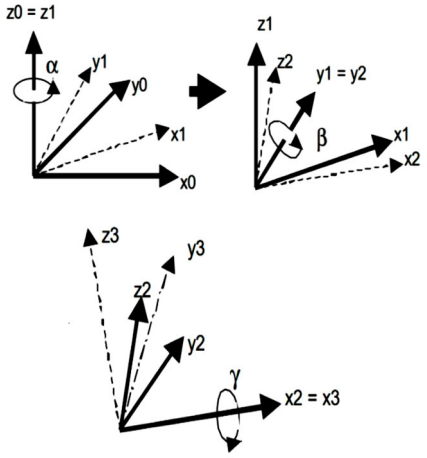

FIGURE 9. Euler angles ZYX (α, β, γ).

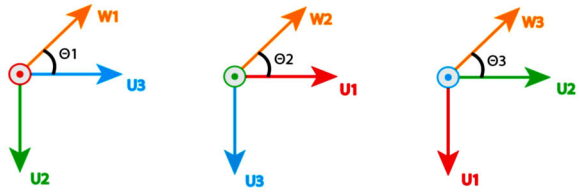

FIGURE 10. Projections of Wi vectors in the fixed frame.

$$\mathbf{V}_3 = \begin{bmatrix} -\cos(\alpha)\cos(\beta) \\ -\sin(\alpha)\cos(\beta) \\ -\sin(\beta) \end{bmatrix} \quad (16)$$

The vectors $\mathbf{W_i}(\theta_i) = [\,\mathbf{W_1}, \mathbf{W_2}, \mathbf{W_3}]$, where θ_i denotes the angles of the motors. Note that W_1 is always in the (O, U_2, U_3) plane, W_2 in the (**O, U_1, U_3**) plane and W_3 in the (O, U_1, U_2) plane as shown in Fig. 10.

The expressions of the vectors $\mathbf{W_i}$ in the fixed frame are therefore:

$$\mathrm{W}_1 = \begin{bmatrix} 0 \\ -\sin\theta_1 \\ \cos\theta_1 \end{bmatrix}, \mathrm{W}_2 = \begin{bmatrix} \cos\theta_2 \\ 0 \\ -\sin\theta_2 \end{bmatrix}, \mathrm{W}_3 = \begin{bmatrix} -\sin\theta_3 \\ \cos\theta_3 \\ 0 \end{bmatrix} \quad (17)$$

To identify the problem and find the equations that relate θ and the angles roll, pitch, yaw XYZ (γ, β, α), the vector

$$\mathbf{R} = \mathrm{R_z}.\mathrm{R_y}.\mathrm{R_x} \quad (9)$$

$$\mathbf{R} = \begin{bmatrix} \cos(\alpha) & -\sin(\alpha) & 0 \\ \sin(\alpha) & \cos(\alpha) & 0 \\ 0 & 0 & 1 \end{bmatrix} . \begin{bmatrix} \cos(\beta) & 0 & \sin(\beta) \\ 0 & 1 & 0 \\ -\sin(\beta) & 0 & \cos(\beta) \end{bmatrix} . \begin{bmatrix} 1 & 0 & 0 \\ 0 & \cos(\gamma) & -\sin(\gamma) \\ 0 & \sin(\gamma) & \cos(\gamma) \end{bmatrix} \quad (10)$$

$$\mathbf{R} = \begin{bmatrix} \cos(\alpha)\cos(\beta) & \cos(\alpha)\sin(\beta)\sin(\gamma) - \sin(\alpha)\cos(\gamma) & \cos(\alpha)\sin(\beta)\cos(\gamma) + \sin(\alpha)\cos(\gamma) \\ \sin(\alpha)\cos(\beta) & \sin(\alpha)\sin(\beta)\sin(\gamma) + \cos(\alpha)\cos(\gamma) & \sin(\alpha)\sin(\beta)\cos(\gamma) - \cos(\alpha)\sin(\gamma) \\ -\sin(\beta) & \cos(\beta)\sin(\gamma) & \cos(\beta)\cos(\gamma) \end{bmatrix} \quad (11)$$

product expressed by (18) is used as follows:

$$W_i.V_i = \cos(\alpha_2) \quad i = 1,\ 2,\ 3 \tag{18}$$

Since α_2 =90°, we find:

$$W_i.V_i = 0 \quad i = 1,\ 2,\ 3 \tag{19}$$

Replacing (14), (15), (16) and (17) in (19), on gets the following system of (20), shown at the bottom of the next page, such as in (20).

A. INVERSE KINEMATICS

The solution of the inverse problem in (20) allows the determination of the motor rotation angles θ_i from the end effectors orientation Roll, Pitch, and Yaw XYZ (γ, β, αInverse kinematics plays a crucial role in the control of manipulators as it enables the determination of the joint angles, denoted as θi, for a given trajectory. Therefore, it can be concluded that:

$$\tan\theta_1 = \frac{\cos\beta.\sin\alpha}{\cos\gamma.\cos\alpha + \sin\gamma.\sin\beta.\sin\alpha} \tag{21}$$

$$\tan\theta_2 = \frac{\sin\gamma.\sin\alpha + \cos\gamma.\sin\beta.\cos\alpha}{\cos\beta.\cos\alpha} \tag{22}$$

$$\tan\theta_3 = \tan\gamma \tag{23}$$

where tan(x) = tan(x+k. π) or k is a natural number.

So, the solutions found are not unique. The manipulator design restricts the possible solutions to the range of -60° to 60° for k=0. In this situation, the solutions are proven to be unique by simulation using CoppeliaSim software [36]).

B. DIRECT KINEMATICS

The solution of the direct problem in the system given by (20) allows the calculation of the end effectors orientation roll, pitch, and yaw XYZ (γ, β, α) from the angles θ_i of the motors. Unlike serial robots, the direct kinematics in SPM is more complex than the inverse kinematics. The straightforward problem was solved by Bonev et al. [12], and the system can be written as:

$$\begin{cases} \sin\alpha(\sin\theta_1\sin\beta\sin\varphi - \cos\beta\cos\theta_1) \\ \qquad + \cos\alpha\sin\theta_1\cos\varphi = 0 \\ \cos\alpha(\cos\theta_2\sin\beta\cos\varphi - \cos\beta\sin\theta_2) \\ \qquad + \sin\alpha\cos\theta_2\sin\varphi = 0 \\ \sin(\theta_3 - \varphi)\cos\beta = 0 \end{cases} \tag{24}$$

In the case of a trivial solution, where cosβ =0, then $\beta = \pm\pi/2$, the geometry of our manipulator limits the Euler angles in the interval [-70°,70°] (calculated in the simulation part with Coppeliasim), which proves that this case is impossible.

For the non-trivial solution, where sin (θ_3 - γ) = 0, so $\theta_3 = \gamma$. Replacing the value mentioned in (24), yields to the following outcomes:

$$\begin{cases} A_1\cos\alpha + A_2\sin\alpha = 0 \\ A_3\cos\alpha + A_4\sin\alpha = 0 \end{cases} \tag{25}$$

Or:

$$\begin{cases} A_1 = \sin\theta_1\cos\theta_3 \\ A_2 = \sin\theta_1\sin\beta\sin\theta_3 - \cos\beta\cos\theta_1 \\ A_3 = \cos\theta_2\sin\beta\cos\theta_3 - \cos\beta\sin\theta_2 \\ A_4 = \cos\theta_2\sin\theta_3 \end{cases} \tag{26}$$

Since cosα and sinα cannot be zero at the same time, (26) yield a zero determinant, such as:

$$A_1A_4 – A_2A_3 = 0 \tag{27}$$

Replacing the values of A_i in (27):

$$\cos\beta\ (q_1\cos\beta + q_2\sin\beta) = 0 \tag{28}$$

Or:

$$\begin{cases} q_1 = \sin\theta_1\cos\theta_2\cos\theta_3\sin\theta_3 - \cos\theta_1\sin\theta_2 \\ q_2 = \sin\theta_1\sin\theta_2\sin\theta_2\sin\theta_3 + \cos\theta_1\cos\theta_2\cos\theta_3 \end{cases} \tag{29}$$

Since cos$\beta = 0$ is impossible, then the solution of (28) is the following:

$$q_1\cos\beta + q_2\ \sin\beta = 0 \tag{30}$$

So, the solution takes the following form:

$$\beta = \tan^{-1}\left(\frac{-q_1}{q_2}\right) \tag{31}$$

Replacing (31) in (26) leads to α, such as:

$$\alpha = \tan^{-1}\left(\frac{-A_3}{A_4}\right) \tag{32}$$

So, for the present manipulator, the solution of the direct problem is expressed by (33), as follows:

$$\begin{cases} \gamma = \theta_3 \\ \beta = \tan^{-1}\left(\frac{-q_1}{q_2}\right) \\ \alpha = \tan^{-1}\left(\frac{-A_3}{A_4}\right) \end{cases} \tag{33}$$

IV. EXPERIMENTAL RESULTS AND DISCUSSION BASED COPELIASIM ENVIRONEMENT

Virtual reality extensively utilized for kinematic and dynamic modeling of robots [31]. These tools provide a secure environment for code testing and enable alterations to be made to the model. Additionally, they facilitate the simulation of intricate settings. Many general-purpose robot simulators allow visualizing and analyzing the kinematics and/or dynamics of a robot. Even free open-source robot simulators like Webots, Gazebo, and CoppeliaSim are available. However, most simulators are not well suited to simulate closed kinematic chains (parallel robots) and require advanced knowledge of the software to do so. Some simulators used to simulate parallel manipulators are special simulators developed specifically for a particular manipulator. Unfortunately, there are no special simulators developed for SPM and very little academic

work on the simulation of spherical parallel manipulators (Fig. 11). The CoppeliaSim software was selected as the robot simulation tool because it seems to be the most suitable for simulating parallel manipulators. The software library has some parallel manipulators (delta robot, Steward Platform). In this study, we will present the solution of the inverse kinematics obtained by the simulation in CoppeliaSim, and then we will compare this solution with the mathematical solution to validate our kinematic analysis, we will present a detection of collisions, which allows us to determine the limit Euler angles of the manipulator.

A. SOLVING THE INVERSE KINEMATICS

The first step of the robot simulation procedure is to create an adequately defined manipulator model in CoppeliaSim, so that the motion simulation of the manipulator model is consistent with the behavior of the physical prototype. To do this, we must first import the CAD assembly of the manipulator into CoppeliaSim as a mesh, 3D object: STL format. The spherical parallel manipulator is a closed chain manipulator. The scene hierarchy encompasses multiple chains. To establish a closed chain, puppet objects are employed to establish connections between the base and the terminal pieces of these chains. There are three chains: the first chain goes from the first actuated joint to the end effectors, the second chain goes from the end effectors to the second actuated joint and the third chain goes from the end effectors to the third actuated joint. The puppet objects connect the second and third chains to the base. To connect each chain to the base, we need two puppet objects: one is the tip associated with the actuated joint that we call the closing tip and the other is the target associated with the base that we call the closing target, and then we connect them by a CI link. We have to define the groups of inverse kinematics; there is only one group of inverse kinematics with three elements: the tip associated with the platform and the two puppet objects associated with the base: closing tip 1 and closing tip 2.

B. COLLISION DETECTION

To add collision detection, it is necessary to designate the specific objects for which the software will do calculations pertaining to collision detection. According to our kinematic analysis, the angles of rotation of the actuated joints (the angles of rotation of the motors) can be expressed as a function of the Euler angles of the platform in the fixed reference frame. The CI equations describe these relationships. It is important to acknowledge that the convention employed for the angles in question is (roll, pitch, yaw), also known as the Euler ZYX convention. The corresponding total rotation matrix for this convention is provided as follows:

$$\mathbf{R} = \mathbf{R}_z(\gamma).\mathbf{R}_y(\beta).\mathbf{R}_x(\alpha) \tag{34}$$

While the convention that CoppeliaSim uses is Euler XYZ, and the total rotation matrix is given by:

$$\mathbf{R} = \mathbf{R}_x(\alpha_c).\mathbf{R}_y(\beta_c).\mathbf{R}_x(\gamma_c) \tag{35}$$

Consequently, it can be concluded that:

- The rotation angles around the **ZYX** axes in the mathematical model are equal to the rotation angles around the **XYZ** axes, respectively, in CoppeliaSim.
- Meanwhile, in CoppeliaSim, the unit vectors of the two references have the same direction, so we have to multiply the Euler angles in CoppeliaSim by (-1).

$$\begin{cases} \alpha_c = -\gamma \\ \beta_c = -\beta, \ \gamma_c = -\gamma \end{cases} \tag{36}$$

A comparison between the calculation validated through virtual reality CopeliaSim software and the real angular position was conducted. The two used configurations shown in Fig. 12 are θ_i^{C1} and θ_i^{C2}. The objective of the comparative analysis is to verify that the robot is able to reach the desired position with high accuracy and to check its repeatability aptitude.

Preliminary tests reveal that the estimated rotation angles for the motors corroborate with the experimental test (Table1). These data confirm the accuracy of the mathematical model and the compliance of the implemented robot. The relative error percentage falls within the range of 2-4%. Part of the error was obtained because the axes of the 9 swivel joints do not coincide perfectly with the center of rotation, so the model is not perfectly isotropic. Still, the deviation of the axes of the joints is negligible, about 0.1 (mm). The majority of the errors are due to the simulation parameters (choice and parameters of gears, the configuration of the joints, etc.). It should be mentioned that, unlike serial manipulators, the joint errors in the manipulators are not cumulative, so if we calculate the real Euler angles, we find them quite close to their theoretical values. For example, we will model a circular trajectory in the Coppeliasim software to obtain the motor rotation angles θ_i. The found angles are transformed into a

TABLE 2. Prototype tests results.

Configuration	Angles	$\theta_{Calculated}$	$\theta_{Measured}$	Error%
$\theta_i^{C_1}$	$\theta_1^{C_1}$	30.01	29.17	2.8
	$\theta_2^{C_1}$	53.4	51.74	3.11
	$\theta_3^{C_1}$	40.38	38.84	3.81
$\theta_i^{C_2}$	$\theta_1^{C_2}$	5.99	5.82	2.84
	$\theta_2^{C_2}$	6.59	6.39	3.03
	$\theta_3^{C_2}$	6	5.86	2.33

$$\begin{cases} -sin\theta_1.(-\cos\alpha.\cos\gamma - \sin\alpha.\sin\beta.\sin\gamma) + cos\theta_1.(-\cos\beta.\sin\gamma) = 0 \\ cos\theta_2.(-\sin\alpha.\sin\gamma - \cos\alpha.\sin\beta.\cos\gamma) - sin\theta_2.(-\cos\beta.\cos\gamma) = 0 \\ -sin\theta_3.(-\cos\alpha.\cos\beta) + cos\theta_3.(-\sin\alpha.\cos\beta) = 0 \end{cases} \tag{20}$$

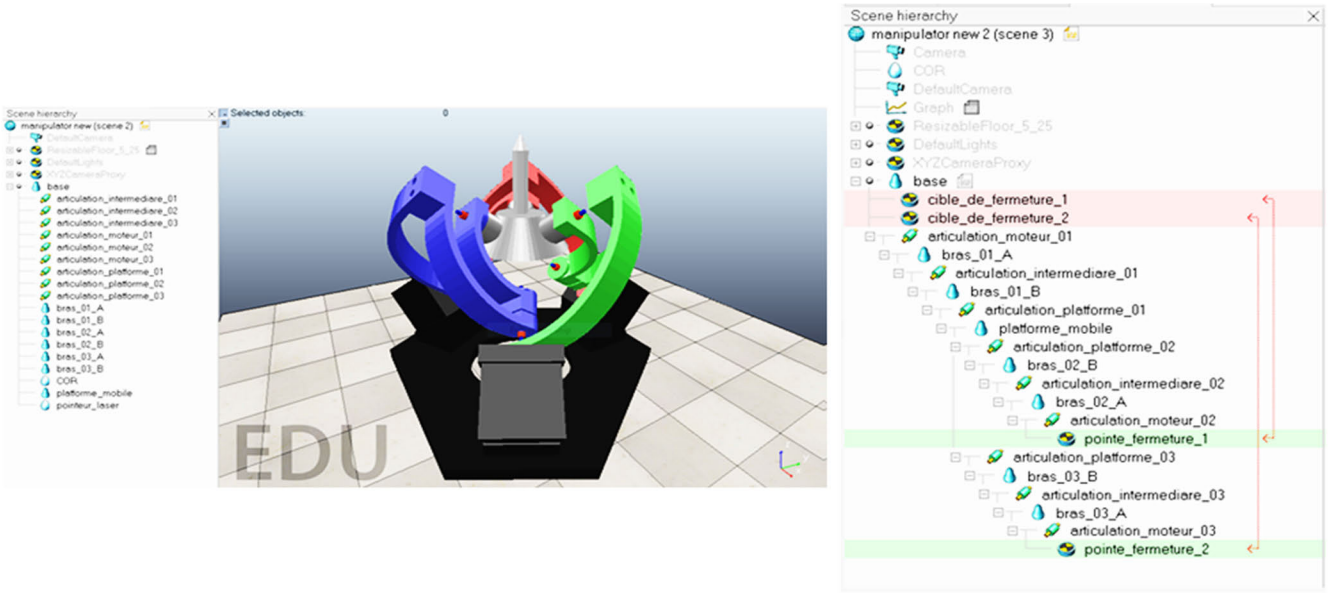

FIGURE 11. Model hierarchy for IC resolution.

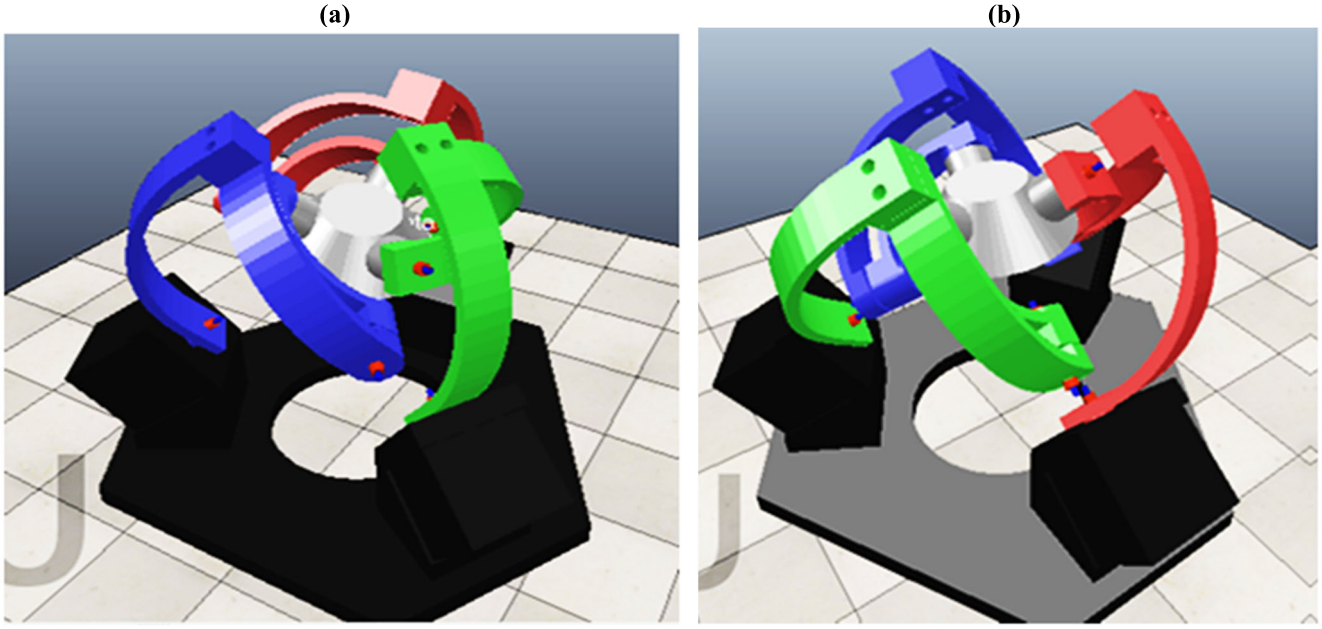

FIGURE 12. Prototype configuration with Euler angles, a) Configuration 1; b) Configuration 2.

Gcode program in order to execute it by the prototype realized via the Mach3 software.

The workspace of the manipulator is a cone of angle equal to twice the angle of inclination $\emptyset_{max}$, more than the height increases more that the opening of the cone increases (Fig. 13). Theoretically, the pointer of the end device (e.g. laser pointer) can draw circles with any radius, it is just necessary to play on the height of the circle position. The maximum height of the circle has a limit so the maximum radius that the manipulator can draw is limited too (Fig. 14). For illustrative purposes, the values R = 1 cm and H = 20 cm were considered as an experimental scenario, as shown in Fig. 15.

C. PATTERN RECOGNITION AND TRACKING

In order to ensure the multifunctioning characteristic of the proposed spherical parallel robot, a visio application is also tested considering two targets. The first scenario was based on virtual reality simulation. In order to make it as universal as possible, two scenarios are tested and programmed. Fistbul, a flyer object detection is performed based on received information from the camera (Fig. 16). It was observed that the robot performs with a high fidelity, with a relative error of 1%. For the second scenario, a human being displacement is introduced (Fig. 17). The virtual reality tests show that the robot could track the human movement with the same accuracy as the first scenario. Such high precision is ensured to the

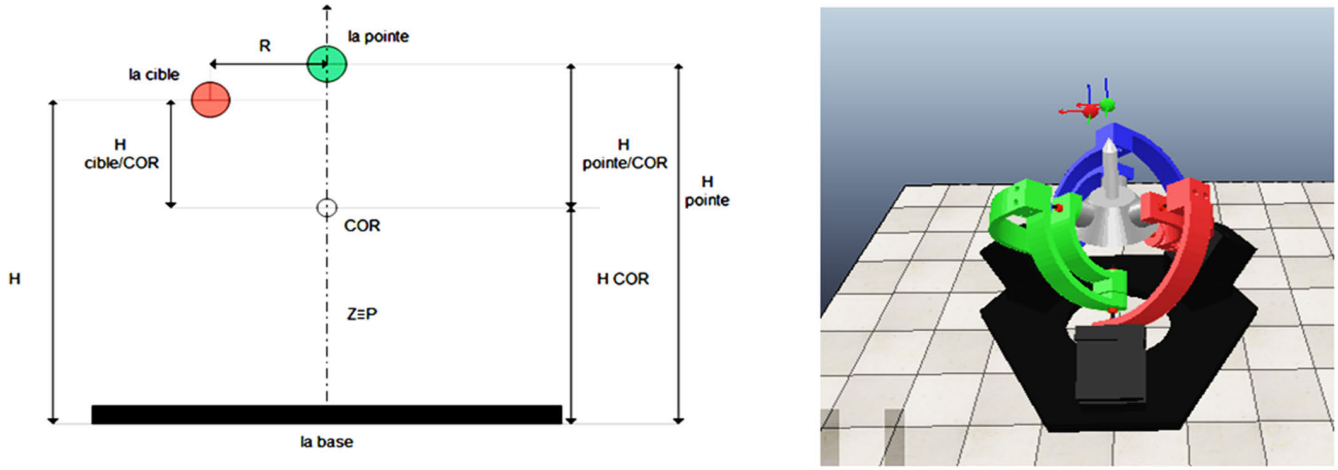

FIGURE 13. Manipulator: initial state.

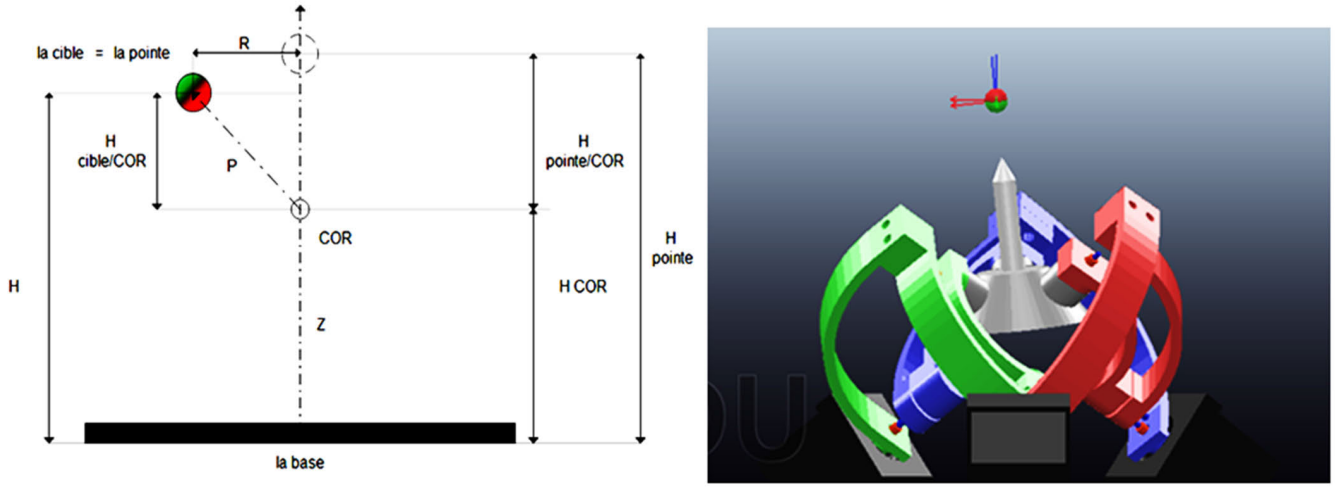

FIGURE 14. Diagram of the manipulator during simulation.

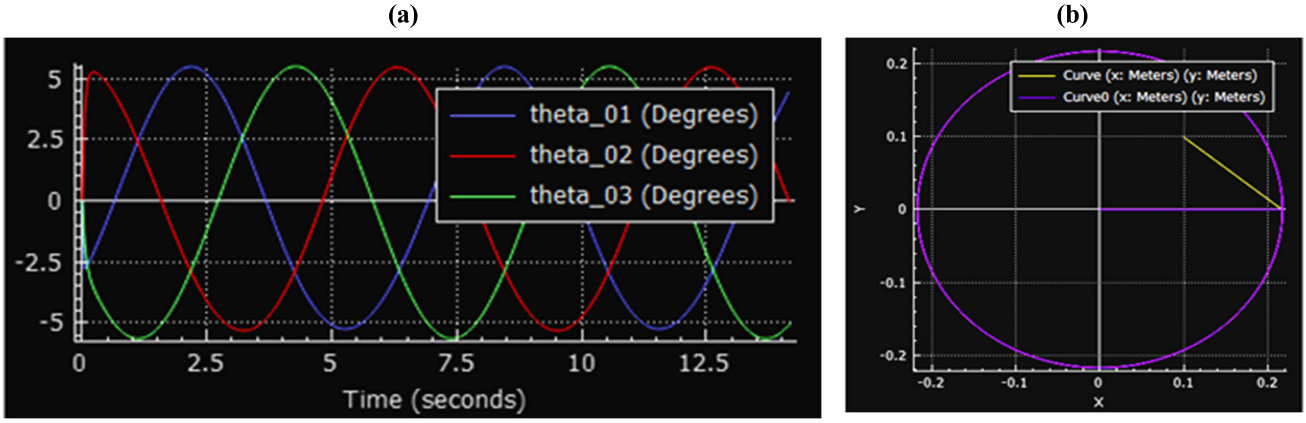

FIGURE 15. Results of a circular trajectory and presentation of the motor angles.

flexible structure of the robot and the important dimensions of the cible objects. In addition, the quality of the used camera ensure a good and redable information.

REMARK 1

All meta-data videos about the conducted tests and virtual reality simulation are accessible via the link below:

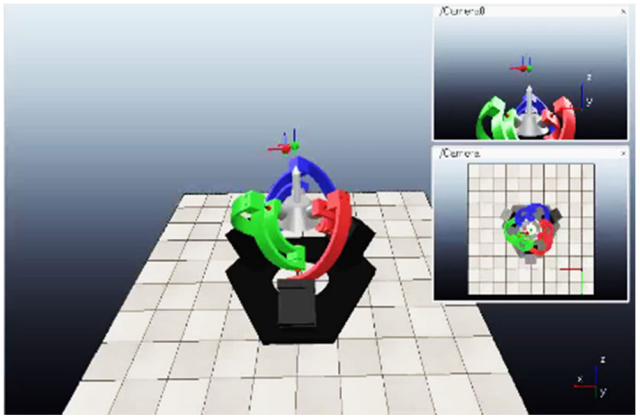

FIGURE 16. 1st scenario of pattern recognition.

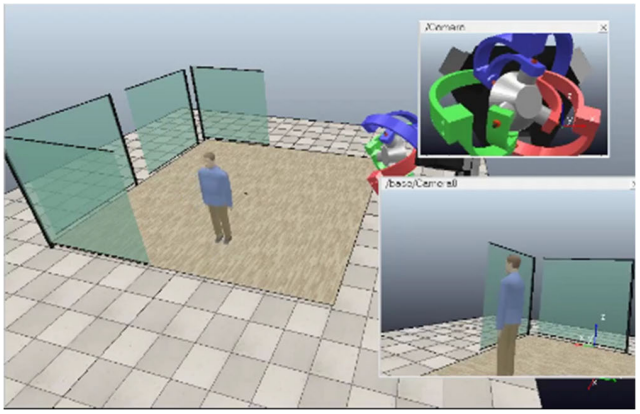

FIGURE 17. 2nd scenario of pattern recognition.

https://drive.google.com/drive/folders/1MId-J09152Gd96WU7TOrKkWrhgRQeEYV?usp=sharing

V. CONCLUSION

Given the importance of robotics and the problems involved in optimizing their precision and repeatability, it is necessary to consider the optimization of both the mechanical architecture and the control system of robots. In this context, this article presents a detailed mechatronic design of a parallel spherical robot with an eagle-eye architecture. The design is functional thanks to the addition of 3-axis motion driven by stepper motors and controlled by a Mach 3 board CNC. The geometry and various construction elements have been optimized to improve the design compared with similar existing robots to enhance and facilitate the assembly/disassembly operation. At the same time, the choice of materials has been carefully considered to lighten the design, reduce energy consumption and ensure that the robot is eco-friendly. To minimize the cost of the development budget, a series of virtual reality experiments based on CoppeliaSim robotics simulator is being used to set the robot in the design phase and during prototype testing by calculating motor rotation angles from well-defined trajectories and to develop control programs in G code. The robot is programmed to execute circular trajectories on a blank sheet of paper using a laser pointer. Minor deviations from the intended direction were seen, as the laser pointer effectively tracked the circular course. The experiments on the experimental prototype prove the efficiency of the robot with a measured error of 0.1 mm and $\pm 0.05°$, thus, 1% for pattern tracking and up to 4% for the circular trajectory tests.

REFERENCES

[1] T. Feng, Y. Yu, L. Wu, Y. Bai, Z. Xiao, and Z. Lu, "A human-tracking robot using ultra wideband technology," *IEEE Access*, vol. 6, pp. 42541–42550, 2018.

[2] Y. Zhang, L. Zhang, W. Wang, Y. Li, and Q. Zhang, "Design and implementation of a two-wheel and hopping robot with a linkage mechanism," *IEEE Access*, vol. 6, pp. 42422–42430, 2018.

[3] C. M. Gosselin and J.-F. Hamel, "The agile eye: A high-performance three-degree-of-freedom camera-orienting device," in *Proc. IEEE Int. Conf. Robot. Autom.*, Aug. 1994, pp. 781–786.

[4] Agile-Eye. (2002). *Laboratoire De Robotique De L'Universite Laval*. [Online]. Available: https://robot: gmc: ulaval: ca/en/research/research-thrusts/parallel-mechanisms/the-agile-eye/

[5] S. Sadeqi, S. P. Bourgeois, E. J. Park, and S. Arzanpour, "Design and performance analysis of a 3-RRR spherical parallel manipulator for hip exoskeleton applications," *J. Rehabil. Assistive Technol. Eng.*, vol. 4, Sep. 2017, Art. no. 2055668317697596.

[6] I. Tursynbek, A. Niyetkaliye, and A. Shintemirov, "Computation of unique kinematic solutions of a spherical parallel manipulator with coaxial input shafts," in *Proc. IEEE 15th Int. Conf. Autom. Sci. Eng. (CASE)*, Aug. 2019, pp. 1524–1531.

[7] D. J. Cox and D. Tesar, "The dynamic model of a three degree of freedom parallel robotic shoulder module," in *Proc. 4th Int. Conf. Adv. Robot.*, 1989, pp. 475–487.

[8] Q. Li, J. M. Hervé, and W. Ye, *Geometric Method for Type Synthesis of Parallel Manipulators*. Cham, Switzerland: Springer, 2020.

[9] J. Gallardo-Alvarado, *Kinematic Analysis of Parallel Manipulators By Algebraic Screw Theory*. Cham, Switzerland: Springer, 2016.

[10] M. Babaiasl. (2022). *Screw Motion and Exponential Coordinates of Robot Motions*. [Online]. Available: https://www: mecharithm: com/screw-motion-and-exponentialcoordinates-of-robot-motions/

[11] O. Mahdizadeh, A. Z. Meymand, M. Mollahossein, and S. A. A. Moosavian, "Kinematics and dynamics modeling of spherical parallel manipulator," in *Proc. 6th RSI Int. Conf. Robot. Mechatronics (IcRoM)*, Oct. 2018, pp. 406–412.

[12] I. A. Bonev, D. Chablat, and P. Wenger, "Working and assembly modes of the agile eye," in *Proc. IEEE Int. Conf. Robot. Autom.*, Oct. 2006, pp. 2317–2322.

[13] M. Arredondo-Soto, E. Cuan-Urquizo, and A. Gómez-Espinosa, "The compliance matrix method for the kinetostatic analysis of flexure-based compliant parallel mechanisms: Conventions and general force-displacement cases," *Mechanism Mach. Theory*, vol. 168, Feb. 2022, Art. no. 104583.

[14] X. Kong and C. M. Gosselin, "A formula that produces a unique solution to the forward displacement analysis of a quadratic spherical parallel manipulator: The agile eye," *J. Mech. Robot.*, vol. 2, no. 4, pp. 1–14, Nov. 2010.

[15] D. Chablat and P. Wenger, "A six degree-of-freedom haptic device based on the orthoglide and a hybrid agile eye," in *Proc. 30th Annu. Mech. Robot. Conf.*, Jan. 2006, pp. 795–802.

[16] A. Cammarata, M. Lacagnina, and R. Sinatra, "Closed-form solutions for the inverse kinematics of the agile eye with constraint errors on the revolute joint axes," in *Proc. IEEE/RSJ Int. Conf. Intell. Robots Syst. (IROS)*, Oct. 2016, pp. 317–322.

[17] C.-H. Kuo, J. S. Dai, and G. Legnani, "A non-overconstrained variant of the agile eye with a special decoupled kinematics," *Robotica*, vol. 32, no. 6, pp. 889–905, Sep. 2014.

[18] I. S. Howard, "Design and kinematic analysis of a 3D-printed 3DOF robotic manipulandum," in *Proc. Annu. Conf. Towards Auto. Robotic Syst.*, 2023, pp. 227–239.

[19] H. Ge, Z. Ying, Z. Chen, W. Zu, C. Liu, and Y. Jin, "Improved A algorithm for path planning of spherical robot considering energy consumption," *Sensors*, vol. 23, no. 16, p. 7115, Aug. 2023.

[20] K. Schröder, G. Garcia, R. Chacón, G. Montenegro, A. Marroquín, G. Farias, S. Dormido-Canto, and E. Fabregas, "Development and control of a real spherical robot," *Sensors*, vol. 23, no. 8, p. 3895, Apr. 2023, doi: 10.3390/s23083895.
[21] L. Zhang, X. Ren, and D. Zheng, "Modeling and control of a new spherical robot with cable transmission," *Int. J. Control, Autom. Syst.*, vol. 21, no. 3, pp. 963–974, Mar. 2023.
[22] Y. Li, M. Yang, B. Wei, and Y. Zhang, "Energy-saving control of rolling speed for spherical robot based on regenerative damping," *Nonlinear Dyn.*, vol. 111, no. 8, pp. 7235–7250, Apr. 2023.
[23] I. H. Sagsoz and T. Eray, "Design and kinematics of mechanically coupled two identical spherical robots," *J. Intell. Robotic Syst.*, vol. 108, no. 2, p. 12, Jun. 2023.
[24] M. A. Arif, A. Zhu, H. Mao, X. Zhou, J. Song, Y. Tu, and P. Ma, "Design of an amphibious spherical robot driven by twin eccentric pendulums with flywheel-based inertial stabilization," *IEEE/ASME Trans. Mechatronics*, pp. 1–13, Mar. 2023.
[25] S. Bu, L. Yan, X. Gao, G. Wang, P. Zhao, and I.-M. Chen, "Design and motion control of spherical robot with built-in four-wheel omnidirectional mobile platform," *IEEE Trans. Instrum. Meas.*, vol. 72, pp. 1–10, 2023.
[26] Y. J. Chen, W.-C. Tung, W.-R. Lee, B. Patel, V. Buč inskas, M. Greitans, and P. T. Lin, "Designing and controlling a self-balancing platform mechanism based on 3-RCC spherical parallel manipulator," *Robotic Syst. Appl.*, vol. 3, no. 1, pp. 1–16, Jun. 2023.
[27] C. M. Gosselin, E. S. Pierre, and M. Gagne, "On the development of the Agile Eye," *IEEE Robot. Autom. Mag.*, vol. 3, no. 4, pp. 29–37, Dec. 1996.
[28] G. Legnani and I. Fassi, "Kinematics analysis of a class of spherical PKMs by projective angles," *Robotics*, vol. 7, no. 4, p. 59, Sep. 2018.
[29] S. Abdelmoeti, *The Viro Agile Eye*, 2018.
[30] G. Wu and S. Bai, "Design and kinematic analysis of a 3-RRR spherical parallel manipulator reconfigured with four–bar linkages," *Robot. Comput.-Integr. Manuf.*, vol. 56, pp. 55–65, Apr. 2019.
[31] A. Alamdar et al., "A modified agile-eye mechanism for robotic manipulation of wristed laparoscopic instruments," *TechRxiv*, Sep. 2021, doi: 10.36227/techrxiv.16602245.v1.
[32] C. Gosselin and J. Angeles, "The optimum kinematic design of a spherical three-degree-of-freedom parallel manipulator," *J. Mech., Transmissions, Autom. Design*, vol. 111, no. 2, pp. 202–207, Jun. 1989.
[33] J. K. Salisbury and J. J. Craig, "Articulated hands: Force control and kinematic issues," *Int. J. Robot. Res.*, vol. 1, no. 1, pp. 4–17, Mar. 1982.
[34] C. Gosselin and J. Angeles, "A global performance index for the kinematic optimization of robotic manipulators," *J. Mech. Des.*, vol. 113, no. 3, pp. 220–226, Sep. 1991.
[35] Y. Shin, H. W. Lim, M. H. Kang, M. Seong, H. Cho, and J. H. Kim, "Normal range of eye movement and its relationship to age," *Acta Ophthalmol.*, vol. 94, no. S256, Oct. 2016.
[36] B. Bogaerts, S. Sels, S. Vanlanduit, and R. Penne, "Connecting the CoppeliaSim robotics simulator to virtual reality," *SoftwareX*, vol. 11, Jan. 2020, Art. no. 100426.

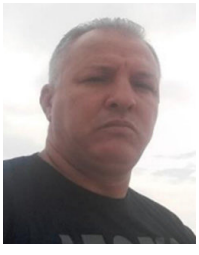

MOHAMED DJENNANE was born in Algeria. He received the Ph.D. degree in mechanical engineering from the University of Batna, Algeria. He is currently an Assistant Professor with the Department of Mechanical Engineering, National Polytechnic Institute of Constantine (École Nationale Polytechnique de Constantine), Algeria. His research interests include machining optimization, industrial robots, and the design of mechanical systems.

SEIF EDDINE CHEHAIDIA was born in Annaba, Algeria, in June 1992. He received the B.Sc., M.Sc., and Ph.D. degrees in electrical engineering from Badji-Mokhtar-Annaba University, Algeria. He is currently an Assistant Professor with the Department of Mechanical Engineering, National Polytechnic Institute of Constantine (École Nationale Polytechnique de Constantine), Algeria. His research interests include mechatronics; power system stability, control, optimization, and renewable energy; artificial intelligence applications; and the design of mechanical systems. He is a Reviewer of *Energy*, *International Journal of Electrical Power and Energy Systems*, IEEE Access, *Energy Science and Engineering* (Wiley), *Periodicals of Engineering and Natural Sciences*, *Engineering, Technology and Applied Science Research*, *Heritage and Sustainable Development*, and *International Journal of Electrical and Computer Engineering Systems*. He was a Reviewer for the 14th IFAC Workshop on Adaptive and Learning Control Systems ALCOS, in 2022.

CHOUITER YAKOUB received the Engineering degree in mechanical engineering from the National Polytechnic Institute of Constantine (École Nationale Polytechnique de Constantine), Algeria. His research interests include mechanical design and mechatronic system design.

KHAWLA MESBAH received the Engineering degree in mechanical engineering from the National Polytechnic Institute of Constantine (École Nationale Polytechnique de Constantine), Algerias. She is currently pursuing the Ph.D. degree with the University of Jijel, Algeria. Her research interests include control systems and signals, power system stability, and renewable energy.

MANSOUR ALJOHANI was born in Jeddah, Saudi Arabia, in May 1986. He received the B.Sc. degree in electrical engineering from Riyadh College of Technology, Saudi Arabia, and the M.Sc. and Ph.D. degrees in electrical engineering from the University of Dayton, USA. He is currently an Assistant Professor with the Department of Electrical and Electronic Engineering Technology, Yanbu Industrial College (YIC), Saudi Arabia. His research interests include control systems and signals, power system stability, and renewable energy.

MOHMED I. MOSAAD (Senior Member, IEEE) is currently an Associate Professor with the Department of Electrical and Electronic Engineering Technology, Yanbu Industrial College (YIC), Saudi Arabia. He is the author of more than 100 high-ranked journals and conference papers. His research interests include power system stability, control, optimization, and renewable energy. He is the Editor-in-Chief of *Yanbu Journal of Engineering and Science*. He is a Reviewer for the IEEE Transaction on Power Delivery, IEEE Transaction on Energy Conversion, IET *Electric Power Application Journal*, *IET Generation Transmission and Distribution Journal*, *IET Journal of Engineering*, *IET System Integration, Journal of Cleaner Production, Electric Power System Components, International Journal of Industrial Electronics and Drives* (IJIED), IEEE Access Journal, *Electric Power System Research, Energies, Alexandria Journal of Engineering, Ain Shams Journal of Engineering, Asian Journal of Control, and International Journal of Energy Engineering* (IJEE).